Journal of
Engineering Sciences
Faculty of Engineering
Assiut University
JES
مجلة
العلوم الهندسية
كلية الهندسة
جامعة أسيوط
journal homepage: http://jesaun.journals.ekb.eg

Assessment of seismic vulnerability of RC frames at the end-of-row of buildings with floor-to-floor alignment using multi-strip analysis MSA

Received 11 April 2022; Revised 3 June 2022; Accepted 3 June 2022

Hossameldeen Mohamed [1]*
Ghada Elyamany [2]

Keywords
Pounding, impact force, RC buildings, fragility functions

Abstract

During earthquakes' excitation, adjacent buildings start vibrating out of phase (in different directions) leading to collisions with each other causing severe damage in a phenomenon known as structural pounding. The proposed study analyses the pounding effects for several case studies representing one of the critical pounding configurations found in the Egyptian buildings taxonomy which is building at the end-of-row of buildings. The multi-strip analysis approach (MSA) using fifty-ground motion records has been adopted to reduce the computational effort required for probabilistic performance assessment. The obtained structural performances of the studied cases, expressed in the form of fragility functions, were compared with the corresponding reference cases (i.e., structures with no adjacent buildings). The results provide insights into the type of failure mechanism that contributes to the global collapse of the studied cases. Fragility functions are also developed for different limit states based on these results to extract further conclusions regarding the overall influence of pounding. Results highlight the main differences between the expected performance of the pounding-involved cases compared to the reference cases. Finally, results indicate the relevance of the pounding effect on the overall performance of the considered cases therefore large-scale seismic risk assessment studies should consider fragility functions accounting for different pounding configurations.

1. Introduction

Limited inhabitable land in highly populated countries such as Egypt leads to the construction of buildings with insufficient separation. During earthquakes, these buildings undergo lateral displacement. For buildings with insufficient gap distance, collisions are inevitable. The collision between adjacent structures, also known as the pounding phenomena, significantly changes the global response of the collided buildings namely the loading path and, therefore, the collapse mechanisms

[1] Assistant professor, Dept. of Civil Engineering, Faculty of Engineering, Aswan University, Hossam.ahmed@aswu.edu.eg
[2] Dept. of Civil Engineering, Faculty of Engineering, Aswan University

https://doi.org/10.21608/JESAUN.2022.132901.1127

[1-3]. Devastating earthquake events leave huge life and economical losses, particularly for those structures with inherited seismic vulnerability. Based on the post-event survey after major earthquakes, adjacent buildings showed a vulnerable performance with excessive damages compared to the individual buildings [4-6]. The observed damage varies from local damages at the contact surface to more severe damages namely shear failure at beams or columns and even the global collapse.

Over 50 years, a vast body of literature addressing the pounding effects on the structural response has been found based on the provided lessons from major earthquakes (e.g., see [1, 7] among others). These studies were found on different scales; from studying the impact phenomena on the global performance of the adjacent structures with a limited number of ground motions [8-11]. In another hand, many research studies were dedicated to determining the optimum safe gap distance between adjacent structures (e.g., see [12-14] among others). Even though these studies provide important conclusions regarding the estimation of the safe distance between the adjacent buildings which can be used for new constructions, still the majority of existing structures were found with no seismic gap. The critical pounding configurations, those with a high probability to experience severe damage due to earthquakes, have been closely studied. These configurations include adjacent buildings exhibiting floor-to-column alignments, adjacent buildings with significant mass or height differences, buildings at the end-of-row of buildings, and buildings likely to experience eccentric pounding [4, 5, 15, 16]. Several types of these configurations are found in Egyptian building taxonomy with a significant number of buildings that can be classified in the category of the building at the end-of-row of buildings. The latter fact is an expected result of the forced-by-law urban rules which correlate the buildings' height to the street width. As such, a two-façade building in conjunction with unequal-width streets is to be adjacent to a lower/higher row of buildings. Still, such configurations have not been studied intensively due to the involved high computational effort.

Studying the seismic performance of existing structures is still a challenge due to the associated uncertainties namely the input ground motions, material parameters, and numerical simulations. Therefore, probabilistic-based earthquake engineering (PBEE) emerged as a comprehensive procedure to assess the performance of existing structures counting for all associated uncertainties. The base idea of PBEE aims not only to confidently improve the structural performance of structures subjected to earthquakes but also to provide a deep understanding of effective seismic risk mitigation measures. However, the high computational effort that is required for PBEE studies limited their use for studies that involved pounding phenomena [1, 2]. As such, a few studies were found to study the adjacent building in the scope of the PBEE. The proposed study addresses the performance of existing adjacent buildings in Egyptian building taxonomy following the PBEE approach by implementing a time-efficient approach. To this end, a series of nonlinear time history analyses were performed on a wide variety of buildings' configurations using a multi-strip analysis (MSA) approach that balances the accuracy and efficiency. These configurations involve reference cases (i.e., with no adjacent buildings) and cases with adjacent buildings that are shuffled to provide six different configurations among three different storeys.

2. **Building Characteristics and the Considered Cases.**

To assess the pounding effect on the RC frames, a 3-bay frame at the exterior axis of a residential building was selected to be a representative case of study. The selected frame has been used as the 2-

D frame with three different numbers of storeys (two-, four-, and six-storey) to simulate different pounding scenarios. The storey height of the considered frame is 3.0 meters and has three-equal spans of 4.3 meters in width. The considered frames have been designed following the Egyptian code provision and regulation [17, 18]. It is worth mentioning that only the gravity loads have been considered in the design process to simulate the scenario of non-seismically designed buildings. As the design inputs, the characteristic values of 25 MPa and 552 MPa have been used for concrete and steel materials, respectively. Accordingly, the columns' sections were found to be 30*30 cm2 with 8 longitudinal steel bars of 12 mm diameter with six per meter evenly distributed stirrups of 6 mm diameter. The sections of the beams were found to be 25*40 with four longitudinal steel bars of 12 mm diameter also with evenly distributed six stirrups per meter with 6 mm diameter. These three frames are used with different arrangements to produce six configurations as shown in **Fig. 1**. As can be seen in **Fig. 1**, all configurations reflect the case of the building at the end-of-row of buildings with floor-to-floor alignment with zero gap distance in between. In these configurations, the building at the end of the row (left-hand side) has been used as a 3-bay frame with the same referred design characterizations. The right-hand side buildings were set as a triplicate version of the control case. Nevertheless, to minimize the computational effort and put more focus on the critical building (i.e., the left-hand side), the extended buildings were set with a fifty percent increase in their designed sections. This increase ensures that the two buildings will have different dynamic characterizations to develop impacts.

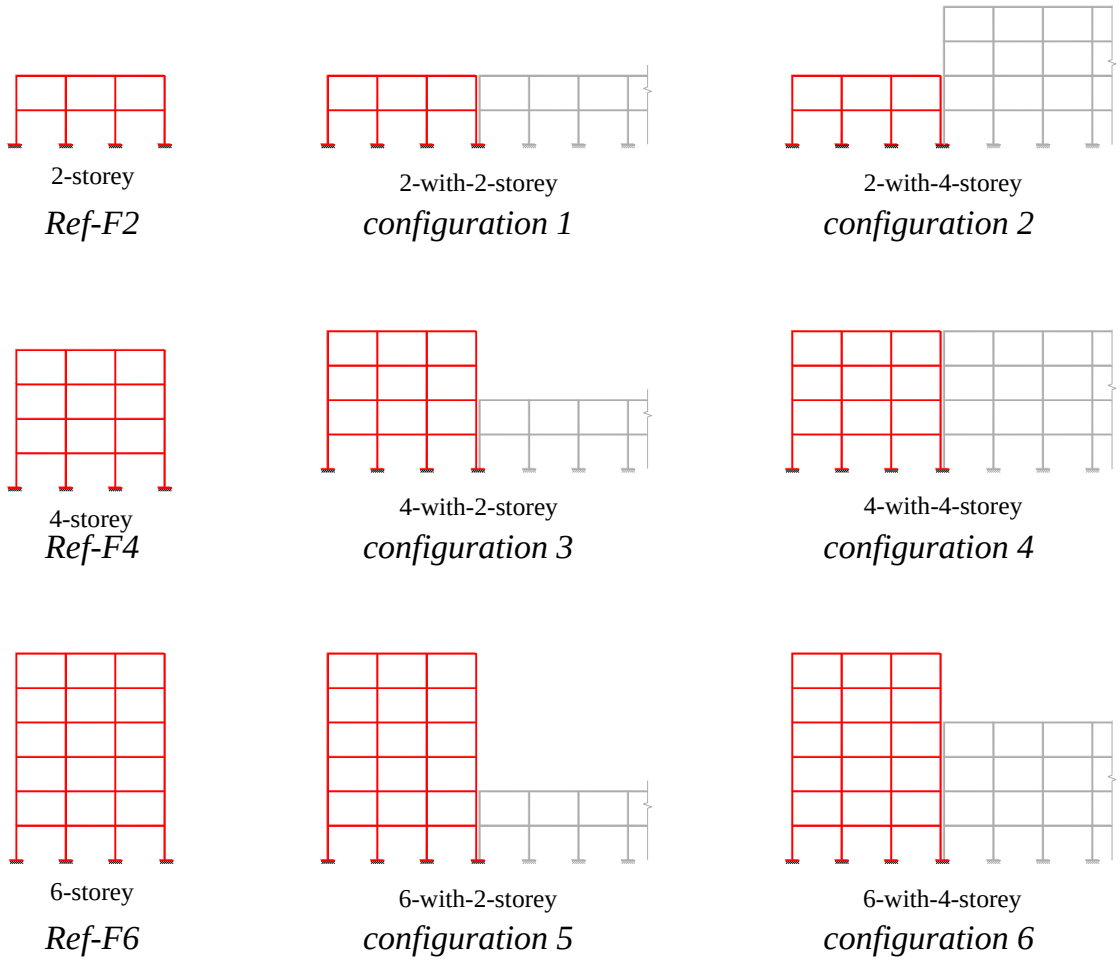

Fig. 1 Considered pounding configurations.

3. Numerical Modelling of RC Elements

The numerical simulations in this research were performed using OpenSees [19]. **Fig. 2 (a)** shows the adopted modelling strategy for the RC elements. As can be seen, both frame's elements (i.e., beams and columns) were modelled using a force-based element. The adopted model is known as the beam With Hinges available in OpenSees element library. Also, **Fig. 2 (b)** shows that beam-column joints were modelled using the rigid-end-offsets approach which allows modelling the connection between the column and beam as a rigid zone. Thus, the joint zone is not considered the flexible part of the elements. The rigid parts' length was assigned according to the dimension of the element to be half of the depth of the perpendicular element as proposed by Mondal and Jain [20]. The locations and weights of the element integration points are based on the plastic hinge integration, which allows the length of the plastic hinges to be determined at the ends of the element. A total of six integration points along the length of the modelled element are used (two for each hinge and two for the middle zone). The integration along the element is based Modified Radau Hinge Integration method [21, 22] which is used to assign the length where the inelastic actions will propagate. Although usually four integration points are used and some studies recommend that using more integration points does not always yield more accurate results [23], in this study, six points have been used to provide a good response in terms of convergence whereas, as will be presented, involving the impact element to the model adds a huge computational effort to reach the convergence. The length of the plastic hinge was determined using an empirically validated relationship for RC elements proposed in [22] as the following:

$$L_p = 0.08\,L + 0.022\,d_b\,f_y \quad (1)$$

Where L is the length of the element in (mm), L_p is the plastic hinge length in (mm), d_p is the diameter of the steel rebars in (mm) and f_y is the steel yield stress in (N/mm^2).

As shown in **Fig. 2 (c),** the sections of the beams and columns were discretized into three different uniaxial materials available in OpenSees; unconfined concrete, confined concrete, and steel materials. The unconfined concrete known as Concrete01 in OpenSees has been used for the concrete cover, while confined concrete known as Concrte02 has been assigned for the concrete. Eventually, bilinear isotropic strain hardening material known as Steel02 in OpenSees has been used for steel parts. The input for the unconfined was estimated using the concrete Kent-Scott-Park concrete material model. This model has degraded linear unloading/reloading stiffness in compression and with no tensile strength capabilities. The confinement factor of the Confined concrete model was considered as presented in [24]. Regarding reinforcing steel fibres in the longitudinal direction, the inputs for Steel02 material were estimated based on the Menegotto and Pinto [25] constitutive law and its improved version [26] including isotropic strain-hardening effect. The resulting hysteretic responses of used materials are presented in **Fig. 2 (d).** It is worth mentioning that the potential shear failure at the column has been monitored at the postprocessing stage. As such, the shear demand has been compared by the capacity of the columns' section and if it is exceeded the analysis stopped and global failure is identified. Finally, it has been assumed that columns' bases are fixed (i.e., the soil-structure interaction SSI has been discarded). The ability of the modelling strategy to realistically capture the real behaviour of RC buildings has been proved in literature (e.g., see [27-29] among others).

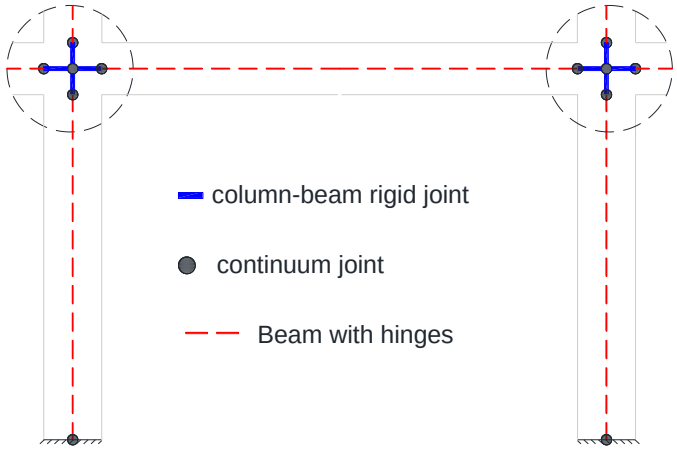

a) General description of the RC elements modelling

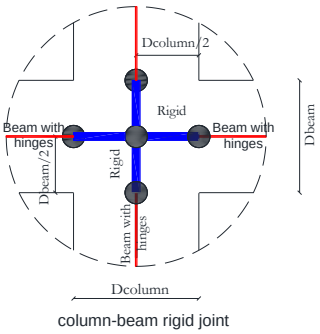

b) Column-beam joint details

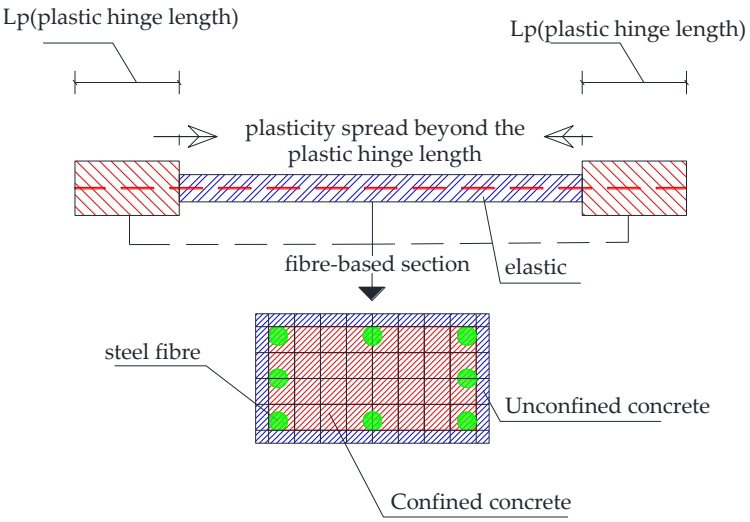

c) Force based beam-column element discretization

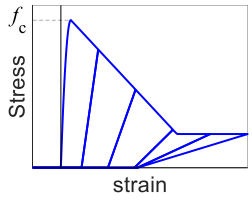

Unconfined concrete material (concrete01)

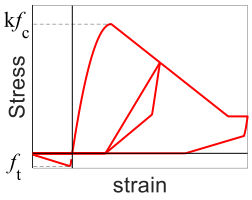

Confined concrete material (concrete02)

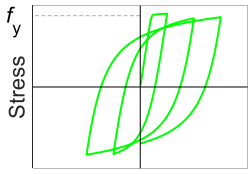

Steel material (steel02)

d) Fibre section materials

Fig. 2 Description of the adopted numerical modelling strategy

4. Numerical Modelling of the İmpact Force

A linear spring with stiffness defined according to the structural characteristics of the contacted buildings combined with the viscous damper model has been used to simulate the pounding between the considered structures at the level of the impact as shown in **Fig. 3**. According to the adopted model which is also known as Kelvin–Voigt model, the pounding force $\overline{F}_p$ is expressed as [30].

$$\bar{F}_p = \begin{cases} \bar{k}(\delta - G) + \bar{c}\,\dot{\delta} & \text{at } \delta > G \\ 0 & \text{at } \delta \leq G \end{cases} \quad (2)$$

Where δ is the relative deformation of colliding the structures, $\dot{\delta}$ is the relative velocity of the colliding structures, G is the gap distance between the colliding structures, $\bar{k}$ and $\bar{c}$ are the impact stiffness and damping, respectively.

To balance the accuracy and efficiency, the lateral stiffness was set to be ten folds of the lateral stiffness of the involved structures [2]. The damping coefficient $\bar{c}$ was estimated based on the value of the coefficient restitution (e) which can be estimated by equating the energy losses during impact [31] which can be driven by the following expressions:

$$\bar{c} = 2\zeta\sqrt{\bar{k}\left(\frac{m_x m_y}{m_x + m_y}\right)} \qquad \text{where } \zeta = -\frac{\ln e}{\sqrt{\pi^2 + (\ln e)^2}} \quad (3)$$

A value of 0.65 was found the most recommended value for the coefficient restitution (e) [32] which corresponds to ζ equals 0.135.

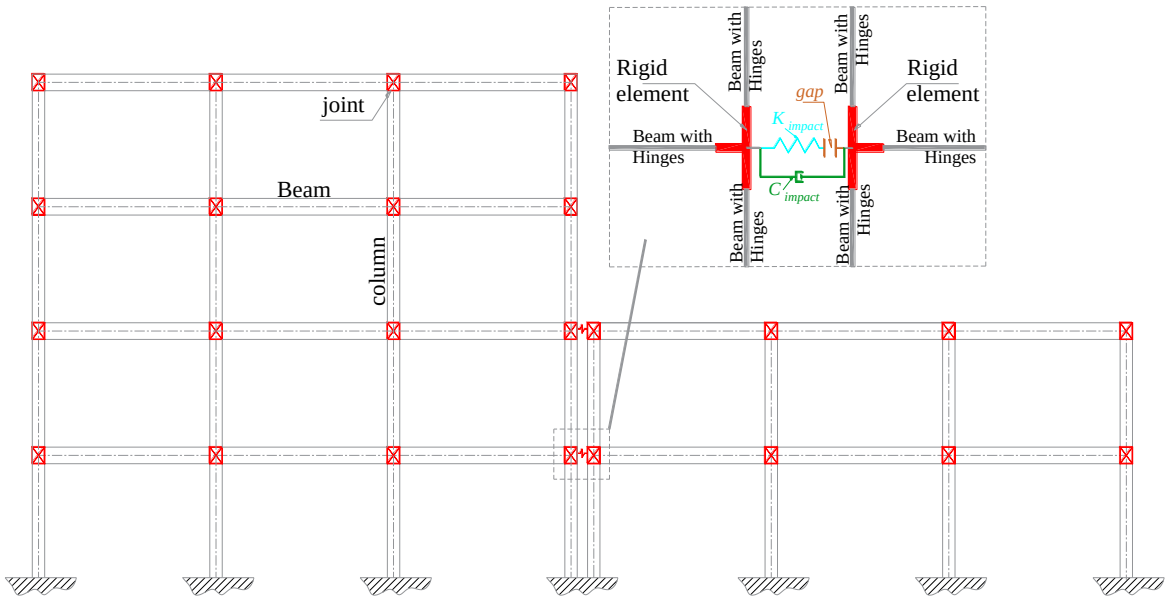

Fig. 3 Modelling description of the contact element

5. Multi-strip Time History Analysis

Given its ability to balance the accuracy and computational efficiency where it requires a smaller number of analyses compared to conventional incremental dynamic analysis (IDA), Multi-strip analysis (MSA) [33-35] was selected as a numerical approach for assessing the performance of the considered cases. In this type of approach, structural analyses were performed at a discrete set of intensity measure IM levels, and different ground motions are used at each IM level. As such, the analyses are not needed to be performed up to the point where all ground motions cause collapse. It

is worth noting that, this type of analysis can involve any number of sets of records including some scaling to make sure that all runs at a given IM level perfectly correspond to the IM level requested, without any tolerance. Since the target for this type of analysis is to develop the fragility function, the distribution of engineering demand parameter EDP given IM is represented at each IM level by the empirical distribution of the EDP results extracted from the analyses. In this context, a series of time history nonlinear analyses are performed using the 50 ground motions that are scaled to different levels to get a reasonable probability of exceedance for each predefined limit state. **Fig. 4** summarises the steps that have been followed to run the MSA.

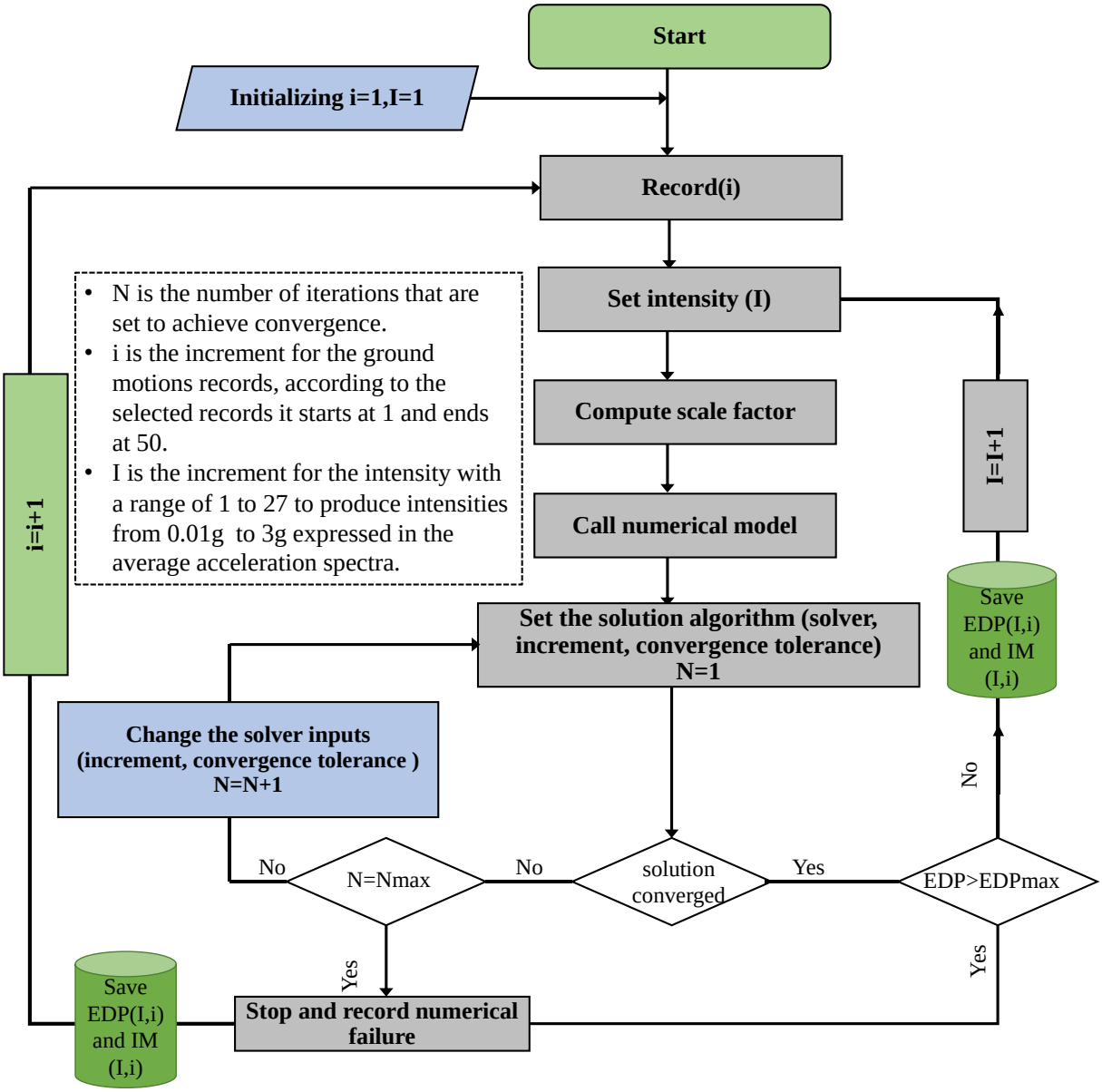

Fig. 4 The overall flowchart describing different steps for the MSA.

6. Ground Motion Records Selection Procedures

In this research, 50 ground motion records that match the target design response spectrum of the Aswan city have been used for the time history analysis. These records were adopted from the PEER's database. The target response spectrum has been defined according to Egyptian code (EC201) which

corresponds to Aswan city, seismic zone3 with peak ground acceleration of 0.15g, medium type of the soil and interpolate seismic action type1. The moment magnitude ranges from 5.74 to 7.62 ML on the Richter scale and the source-to-site distance from 12.35 to 101.62 km. The record selection has been carried out using the software SelEQ platform [36] and properly scaled to fit the EC201 elastic spectra for the period range between 0.15 and 1.5. This range was selected to be compatible with all considered configurations. As shown in **Fig. 5**, the mean response spectrum was found compatible with the target elastic repose for Aswan city.

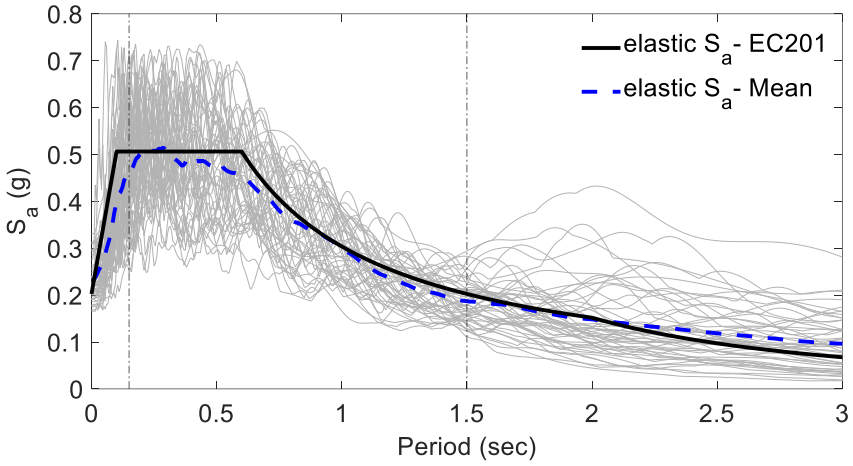

Fig. 5 Target elastic design response spectrum for Aswan city along with the scaled spectra for the fifty ground motions and the mean response spectrum of the selected ground motions.

7. Engineering demand parameters (EDP), damage limit state (DLS) and intensity measure IM

Engineering demand parameters (EDPs) are response quantities that can be interpreted to a physical meaning (i.e., damage state). Several response quantities such as Inter-storey drift, top displacement or floor acceleration are frequently used to characterise demand variation on structures subjected to seismic loading by correlating structural response and ground motion intensity measures (IM). However, several studies have found that the maximum inter-storey drift ratio (IDR_{max}) is indicative of both global structural and non-structural damage in RC buildings [37, 38]. Several proposals were found to define the corresponding damage state for each EDPs [39-41]. In this study, the performance is defined in terms of the maximum inter-storey drifts ratio (IDR_{max} %). The limit states proposed by Rossetto and Elnashai [42] and presented in Table 1 were used. For the IM there are many candidates such as peak ground acceleration (PGA), 5% damped first-mode spectral acceleration, Sa(T1) or 5% damped first-mode spectral displacement, and Sd(T1) [43]. A far better IM candidate is the average spectral acceleration [44] which is given as follows:

$$Sa_{aver} = \left[\prod_{i=1}^{N} S_a(T_i)\right]^{\frac{1}{N}} \quad (4)$$

Where Sa_{aver} is the geometric mean of multiple spectral ordinates $Sa(T_i)$ within a range of the considered periods.

Table 1: Limit state inter-storey drifts proposed by Rossetto and Elnashai [42]

Damage state	Inter-storey drift (%)	Damage state description
DS1	0.05	Slight
DS2	0.08	Light
DS3	0.3	Moderate
DS4	1.15	Extensive
DS5	2.8	Partial collapse
DS6	>4.36	Collapse

8. Results and Discussions

8.1 Time history response

To make the considered building experience different states of damage, a series of time history analyses have been performed with different intensities of the selected ground motions. For each analysis, the maximum inter-storey drift (IDR_{max} %) has been recorded. As aforementioned that adjacent buildings develop different dynamic responses compared to the individual structures, therefore, it is worth comparing the response of the pounded building with the individual structure (control case). **Fig. 6** presents the time history response expressed as the inter-story drift for 6-storey, configuration no.5, and configuration no.6 models under the ImperialValley-02 earthquake (one of the selected records that are compatible with the target response spectrum) at the intensity that leads to the collapse. It is worth noting that the maximum inter-storey drift was calculated using the following equation.

$$IDR_{max}\ (\%) = \frac{|d_j - d_{j-1}|}{\text{storey height}} \times 100 \quad (5)$$

where d is the maximum displacement at the storey j level with respect to the lower floor (j-1). As can be seen in **Fig. 6** that the response of each storey has been recorded for the three models. It is clear that the failure of Ref-F6 (control case) commenced at the first two floors while configurations 5 and 6 failed at the second two floors (i.e., 3S and 4S) and the third two floors (i.e., 5S and 6S), respectively. As such, it can be concluded that pounding leads to shifting the failure of building above the pounding level. In other words, pounded buildings might fail due to forming the critical floor above the level of the contact.

8.2 Maximum inter-storey drift profile

For a better representation of the time history response of the drift, **Fig. 7** presents the IDR_{max} profile for the selected models that were subjected to the ImperialValley-02 earthquake at failure intensity. The drift profile represents the distribution of storey drifts over the building height with respect to IM. The IDR_{max} for each storey was plotted along the abscissa, and the storey was plotted along the ordinate. According to the graph in **Fig. 7**, it can be concluded that for the individual structures (control cases), the mechanism that leads to the collapse commences at the lower floor (following the first vibration mode). The forming of a weak floor at the bottom floor for the control cases is consistent with the fact that the considered structures are not designed for seismic actions (no capacity design is considered). On another hand, for the pounded structures, pounding amplifies the maximum inter-storey drifts for the floors above the contact level (at the top level of the shortest building).

However, for the building with a similar height (i.e., configuration 4), the drift profile has not been affected.

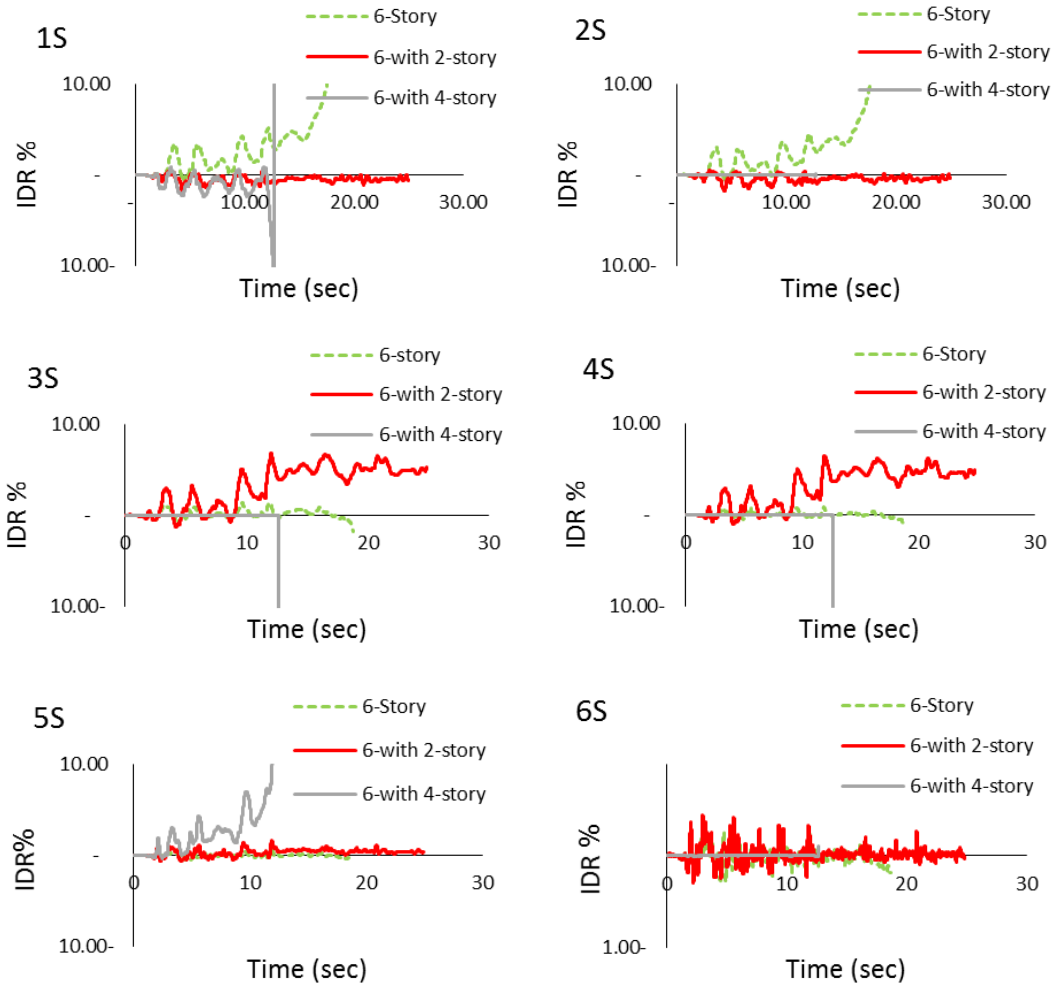

Fig. 6 Comparative drift time histories for pounding and no pounding cases at the failure intensity during ImperialValley-02earthquake. Where 1S, 2S etc., refer to the number of storey i.e., 1S refers to IDR at the first storey.

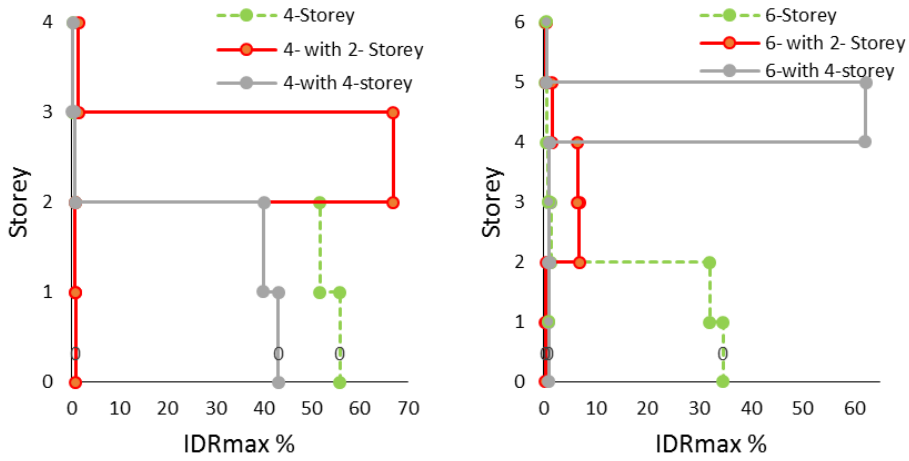

Fig. 7 Comparative IDR_{max} (%) profile for the selected models, plotted for ImperialValley-02 earthquake at failure intensity.

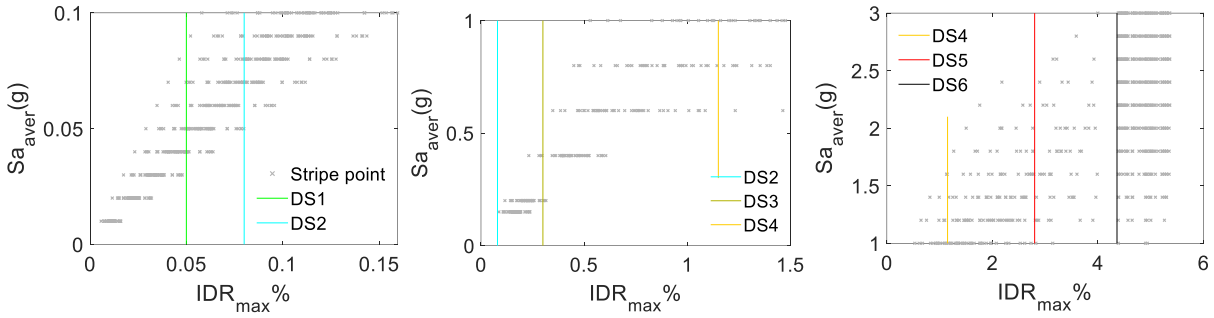

a) Ref-F2

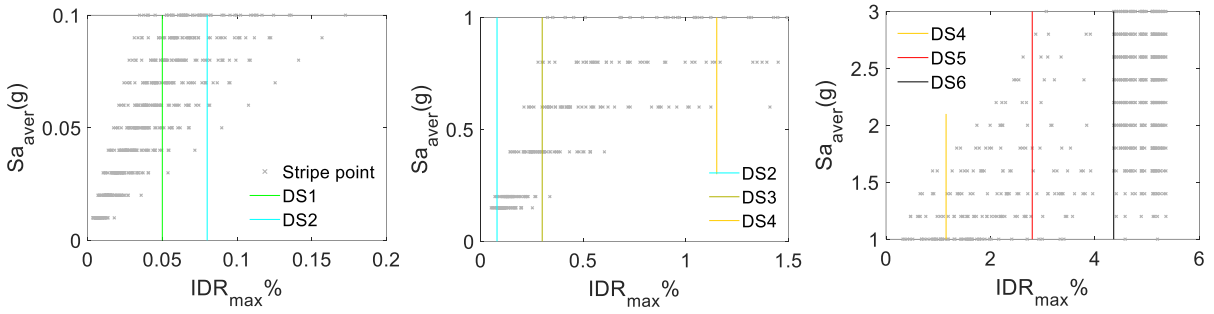

c) Configuration 1

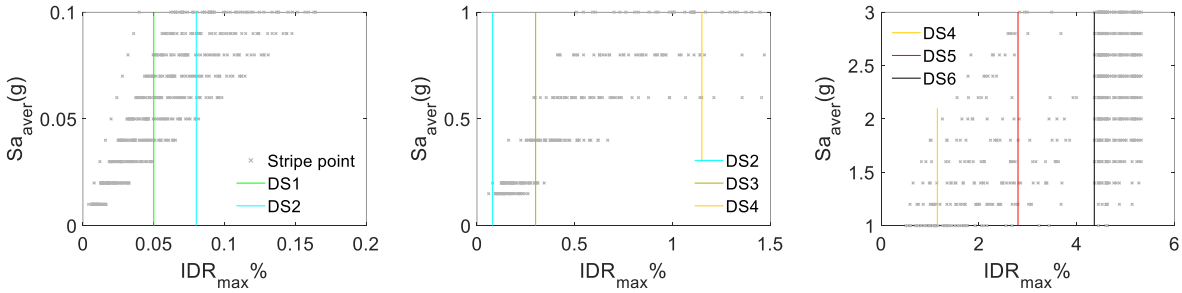

d) Configuration 2

Fig. 8 The results of MSA analyses showing average spectrum acceleration versus interstorey drift for cases that involved a 2-storey frame

8.3 Results of the MSA analyses

According to the referred modelling strategy, nine structures with different configurations were analysed. These involve three individual structures consisting of 2-, 4-, and 6- storey and six pounded structures with different configurations. The multi-stripes analysis (MSA) was performed for all models using 50 ground motion records with twenty-seven different intensities that have a range of Sa_{aver} from 0.01g to 3g. That range has been identified to ensure that all considered buildings experienced all damage states with enough data that is required for fragility curves. In a general sense, the relationship between IDR_{Max}, and IMs (expressed as Sa_{aver}) is represented by the scatter plot (stripes curves) in **Fig. 8**, **Fig. 9,** and **Fig. 10** for 2-,4-and 6-storey buildings, respectively. It is worth noting the stripes have been split into three parts to highlight value at the low IM value. Moreover, the six predefined limit states of damage have been plotted at their corresponding drift values to have a better visualization of the proportion of ground motions that exceed each damage threshold. As can

be seen, the six-storey buildings reach to limit state at low values of IM compared to two and four storeys which reflect the fade of the considered overstrength for these cases due to the increase of the gravity loads. Even though stripes curves provide an overall view of the performance, the fragility curves provide a better representation to assess the performance and compare the different structures.

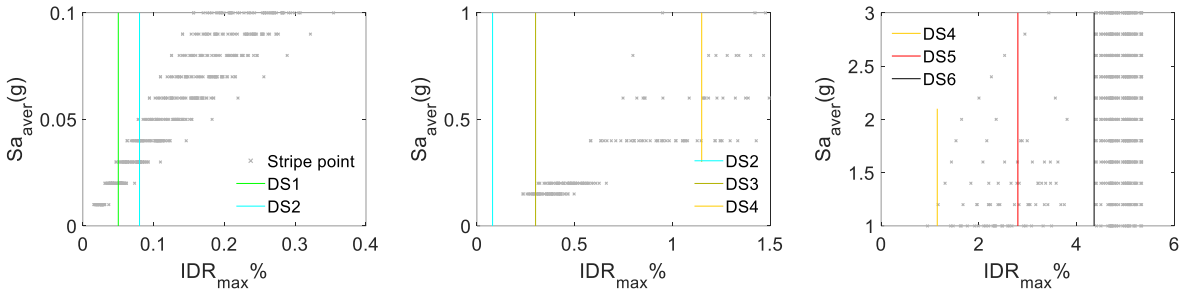

a) Ref-F4

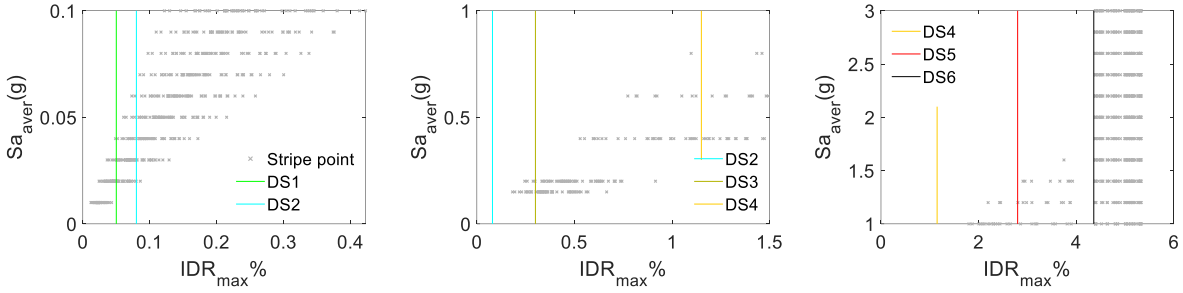

b) Configuration 3

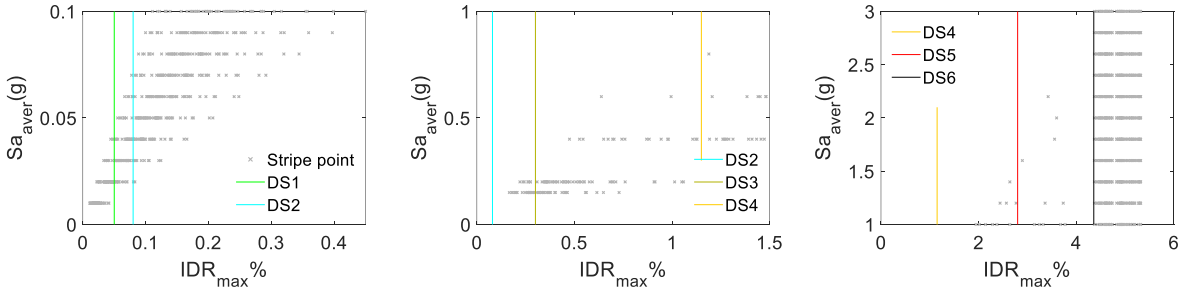

c) Configuration 4

Fig. 9 The results of MSA analyses showing average spectrum acceleration versus interstorey drift for cases that involved a 4-storey frame

To define the fragility cures based on the obtained stripes, the probability of exceedance of a given limit state is quantified at each strip as shown in **Fig. 11**. The cumulative probabilities are then plotted along with their corresponding IM to form what is commonly called empirical or observed fragility data. To get the theoretical fragility function, the theoretical model (herein lognormal cumulative distribution function CDF) minimizes the sum of squared errors (SSE) between the observed fractions of collapse (exceedance of a given limit state) and probabilities of collapse predicted by the fragility function. Using the lognormal cumulative function which provides an adequate accuracy to represent the empirical data [45], the parameters of the fragility curve can mathematically be expressed as:

$$\{\theta, \beta\} = \arg\min_{\theta,\beta} \sum_{j=1}^{m} \left(\frac{z_j}{n_j} - \Phi\left[\frac{\ln(x_j) - \ln(\theta)}{\beta} \right] \right)^2 \quad (6)$$

Where z_j is the observing number of exceedance of a given damage state out of n_j ground motions with IM = x_j, θ and β are the median and standard deviation of the lognormal distribution, respectively. By applying the aforementioned procedures for all limit states for all considered configurations, the fragility parameters θ and β for each limit state is reported in **Table 2.**

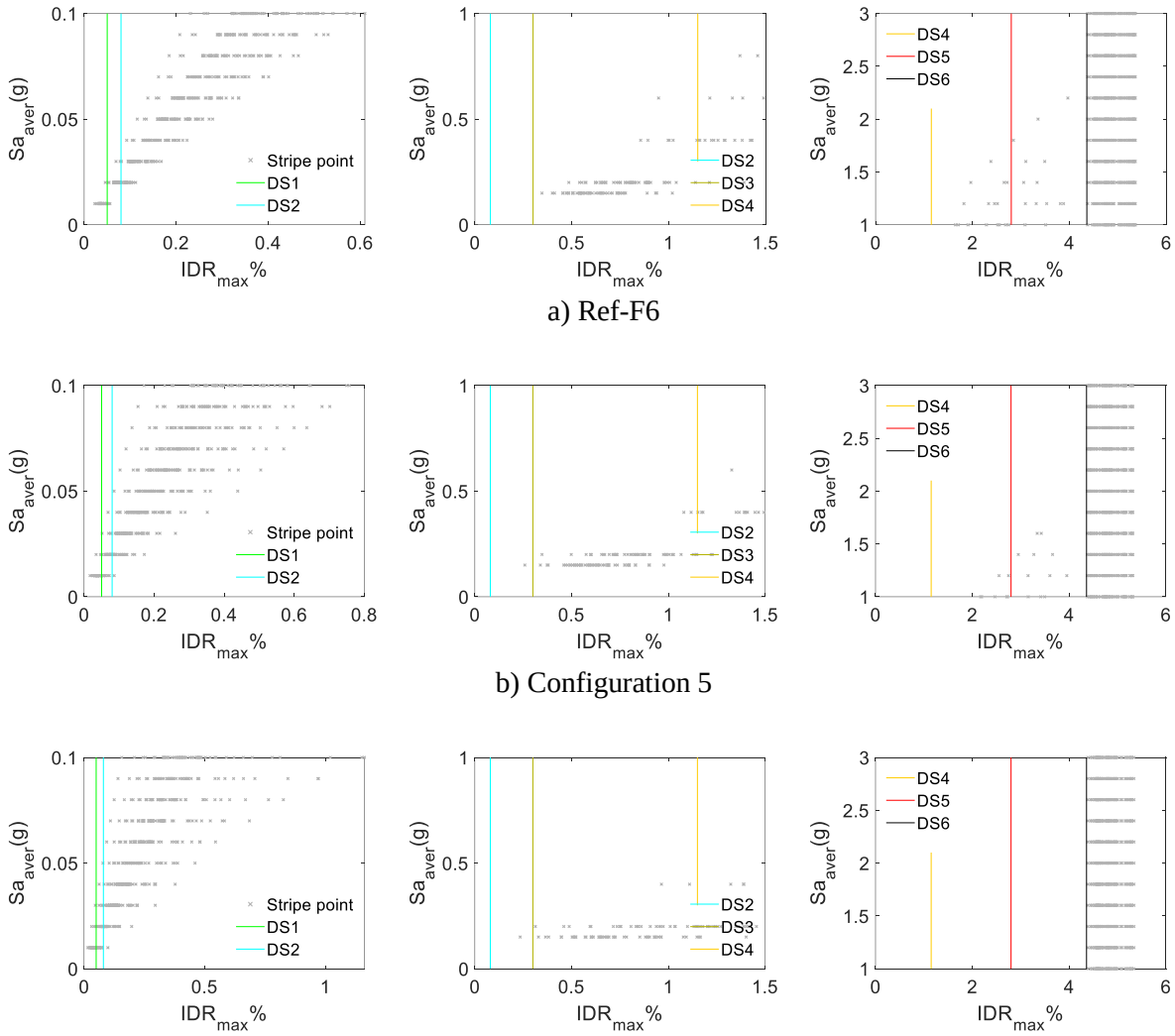

a) Ref-F6

b) Configuration 5

c) Configuration 6

Fig.10 The results of MSA analyses showing average spectrum acceleration versus interstorey drift for cases that involved a 6-storey frame

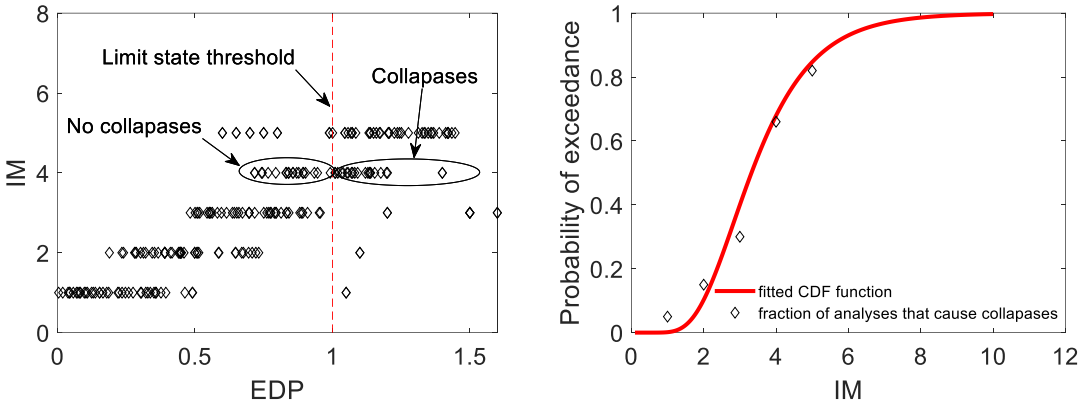

Fig.11 Example of postprocessing of the data obtained from MSA analysis

Table 2: The obtained value of the median (θ) and the standard deviation of the fragility curves for the considered cases at different levels of damage states

model	Slight		Light		Moderate		Extensive		Partial collapse		Collapse	
	θ	β	θ	β	θ	β	θ	β	θ	β	θ	β
Ref-F2	**0.0458**	**0.240**	**0.0732**	**0.239**	**0.4861**	**0.276**	**0.9084**	**0.253**	**1.4298**	**0.282**	**1.6460**	**0.293**
Configuration 1	**0.0673**	**0.361**	**0.1073**	**0.353**	**0.6209**	**0.348**	**0.9693**	**0.257**	**1.4347**	**0.302**	**1.6319**	**0.299**
Configuration 2	**0.0510**	**0.334**	**0.0824**	**0.269**	**0.5229**	**0.325**	**0.9705**	**0.318**	**1.5286**	**0.347**	**1.6615**	**0.361**
Ref-F4	**0.0200**	**0.232**	**0.0333**	**0.236**	**0.2129**	**0.204**	**0.4767**	**0.290**	**0.9321**	**0.417**	**1.0972**	**0.401**
Configuration 3	**0.0209**	**0.297**	**0.0346**	**0.275**	**0.2086**	**0.271**	**0.4256**	**0.315**	**0.8394**	**0.249**	**0.9973**	**0.251**
Configuration 4	**0.0241**	**0.291**	**0.0372**	**0.332**	**0.2166**	**0.303**	**0.3530**	**0.303**	**0.7081**	**0.306**	**0.8010**	**0.361**
Ref-F6	**0.0133**	**0.200**	**0.0214**	**0.192**	**0.1254**	**0.217**	**0.3016**	**0.307**	**0.5757**	**0.518**	**0.6601**	**0.559**
Configuration 5	**0.0120**	**0.290**	**0.0198**	**0.330**	**0.1188**	**0.298**	**0.2723**	**0.220**	**0.5820**	**0.415**	**0.6449**	**0.483**
Configuration 6	**0.0129**	**0.360**	**0.0201**	**0.357**	**0.1136**	**0.307**	**0.2126**	**0.361**	**0.3735**	**0.271**	**0.4843**	**0.312**

8.4 Fragility functions

To assess the effect of pounding on the overall performance of the considered cases, the fragility curves for the cases that involve pounding were compared to their corresponding reference cases. **Fig. 12, Fig. 13, and Fig. 14** show the fragility curve for the reference cases along with their corresponding bounded cases at different limit damage states for two-, four-, and six-storey buildings. In a general sense, pounding does not have a significant negative effect in configurations no.1, no.2, and no.4 for the first three limit state where the structures exposed to pounding exhibit better performance than individual structures for all damage states. That is more prominent for the cases with a similar number of storeys (i.e., configurations 1 and 4), where the bounded cases have a prominent better performance for the first limit state. However, the performance for these configurations is worsened for the higher limit state, particularly for the four-storey buildings which are consistent with Cole, Dhakal [15] observations.

For the buildings with six-storey, even though the bounded cases experience better performance at low seismic demand (lower tail), for the higher seismic demand, the bounded cases experience a fragile performance (higher tail). For the higher limit damage states, the bounded buildings experience more vulnerable performance. This vulnerable performance can be interpreted in light of

the plot that showed that bounded cases are most likely to develop a weak storey above the pounding level. Therefore, the chances of having collapse are increased for the bounded cases. Eventually, it can be concluded that for the considered cases, pounding can lead to a higher percentage of collapse for the buildings with no seismic design, particularly those with a high number of storeys. However, more cases should be investigated with different pounding configurations that involved buildings with seismic design.

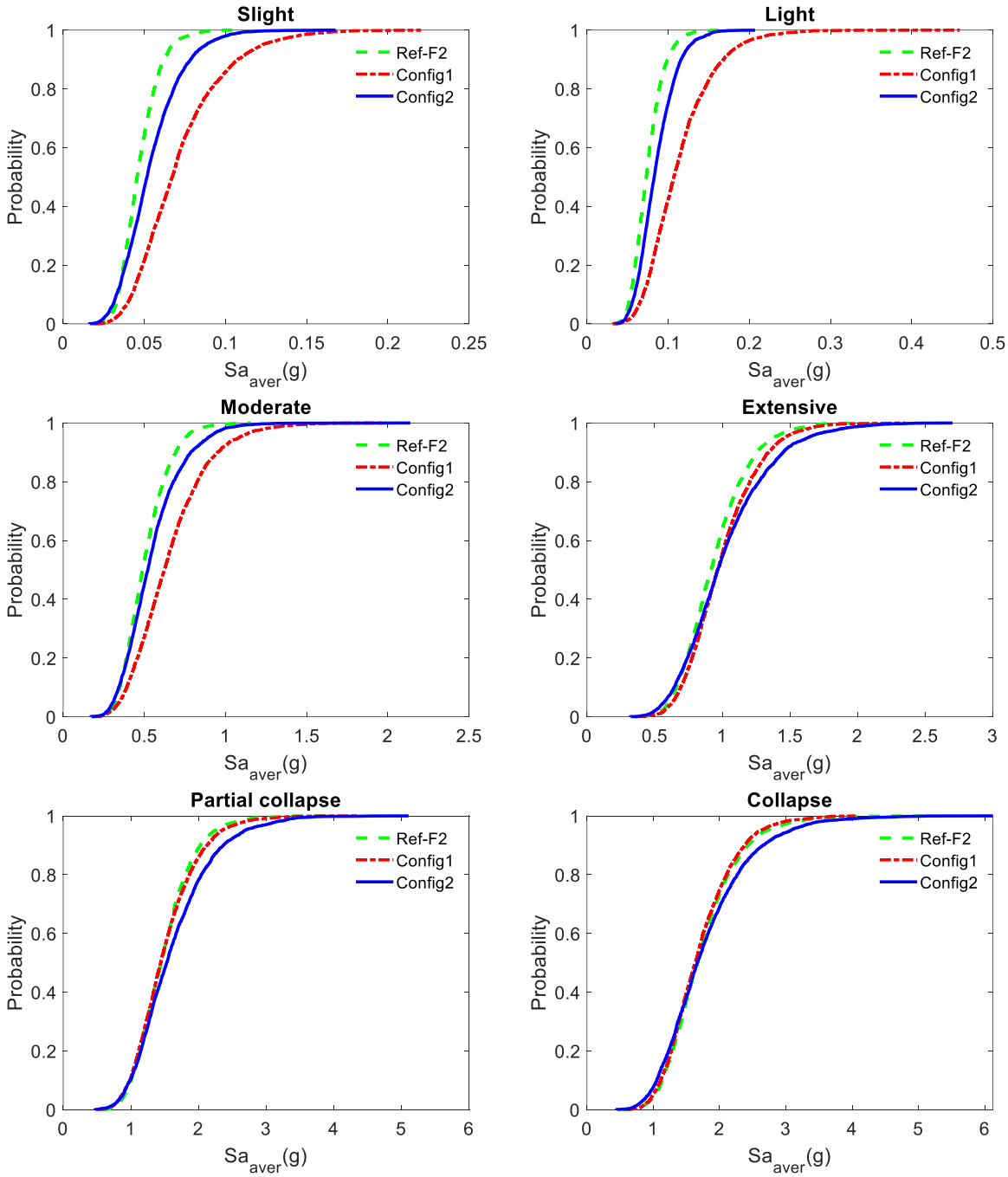

Fig. 12 Fragility curves for configurations of two-storey frames at different limit state definitions

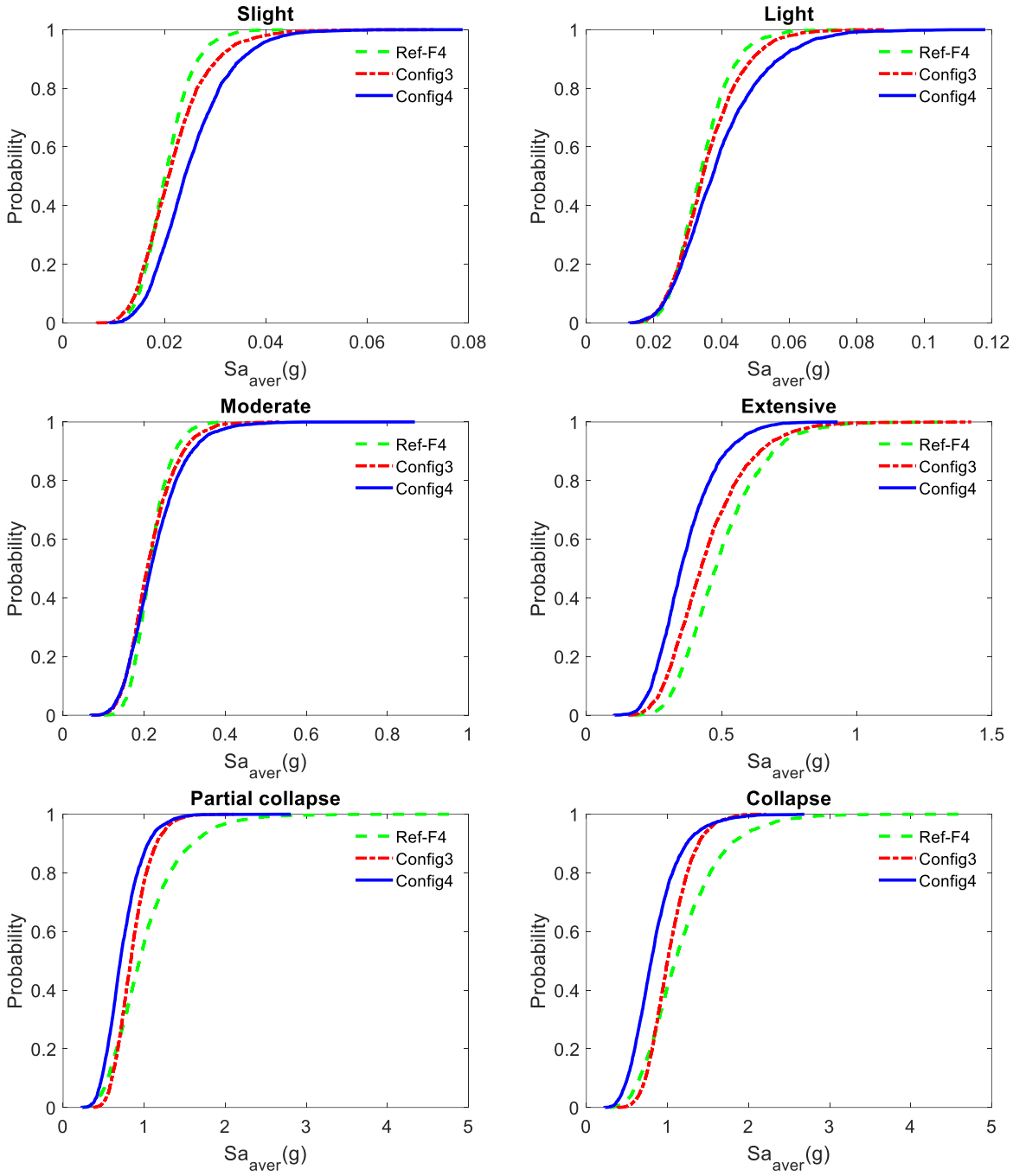

Fig. 13 Fragility curves for configurations of four-storey frames at different limit state definitions

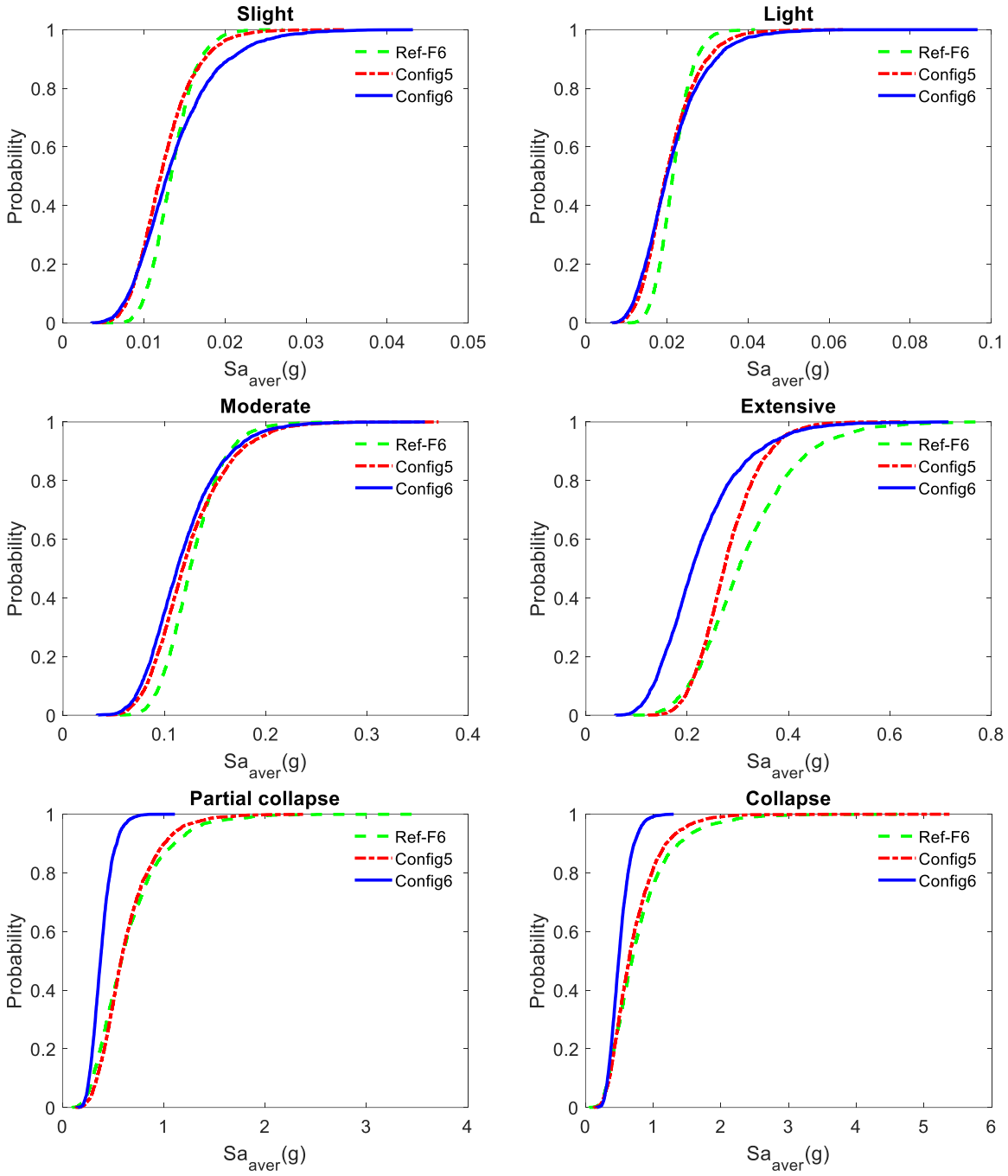

Fig. 14 Fragility curves for configurations of six-storey frames at different limit state definitions

9. Conclusion

The present paper studies the seismic performance of RC frames located at the end-of-row building using multiple stripes analysis. The seismic assessment was carried out through the selection of frames with three different numbers of storeys (two, four, and six storeys) as a control case. These four frames were used with different arrangements to produce six combinations to simulate different pounding scenarios. The behaviour of the structures was analysed by multi-strip analysis using fifty real ground motions records to simulate the seismic scenario which corresponds to seismic zone 3 of Egyptian territory. To evaluate the effect of the pounding, the response of buildings with and without

pounding was compared in terms of failure mechanism and fragility curves. The performance of the structures was then examined for different limit states and vulnerability was then represented by fragility curves. The obtained results showed that pounding between adjacent RC frames can lead to forming a critical floor failure mechanism that leads to global collapse. On another hand, fragility curves showed the building with similar height experienced a closer performance to the corresponding control cases, particularly for the lower limit states (i.e., a minor effect due to pounding). However, for the higher limit states and cases involving four storeys and six storeys, the effect of pounding is prominent. Eventually, the authors recommend using risk mitigation measures for pounding-prone buildings such as using sufficient separation distance for the newly constructed buildings or using proper strengthening techniques for the existing buildings.

References

[1] Mohamed, H., G. Elyamany, and K. Ehab, *Seismic pounding between adjacent building: a review.* Academic Platform Journal of Natural Hazards and Disaster Management, 2021: p. 16-28.

[2] Mohamed, H. and X. Romão, *Seismic Fragility Functions for Non-Seismically Designed RC Structures Considering Pounding Effects.* Buildings, 2021. **11**(12): p. 665.

[3] Kazemi, F., B. Mohebi, and R. Jankowski, *Predicting the seismic collapse capacity of adjacent SMRFs retrofitted with fluid viscous dampers in pounding condition.* Mechanical Systems and Signal Processing, 2021. **161**: p. 107939.

[4] Cole, G.L., R.P. Dhakal, and F.M. Turner, *Building pounding damage observed in the 2011 Christchurch earthquake.* Earthquake Engineering & Structural Dynamics, 2012. **41**(5): p. 893-913.

[5] Shrestha, B. and H. Hao, *Building Pounding Damages Observed during the 2015 Gorkha Earthquake.* Journal of Performance of Constructed Facilities, 2018. **32**(2): p. 04018006.

[6] Sołtysik, B. and R. Jankowski, *Building damage due to structural pounding during earthquakes.* Journal of Physics: Conference Series, 2015. **628**(1): p. 012040.

[7] Kharazian, A. and F. López-Almansa, *State-of-the-Art of Research on Seismic Pounding Between Buildings with Aligned Slabs.* Archives of Computational Methods in Engineering, 2019. **26**(2): p. 327-345.

[8] Raheem, S.E.A., et al., *Seismic pounding effects on adjacent buildings in series with different alignment configurations.* Steel and Composite Structures, 2018. **28**(3): p. 289-308.

[9] Raheem Shehata, E.A., et al., *Seismic pounding between adjacent buildings considering soil-structure interaction.* Earthquakes and Structures, 2021. **20**(1): p. 55-70.

[10] Miari, M., K.K. Choong, and R. Jankowski, *Seismic pounding between adjacent buildings: Identification of parameters, soil interaction issues and mitigation measures.* Soil Dynamics and Earthquake Engineering, 2019. **121**: p. 135-150.

[11] Miari, M., K.K. Choong, and R. Jankowski, *Seismic Pounding Between Bridge Segments: A State-of-the-Art Review.* Archives of Computational Methods in Engineering, 2021. **28**(2): p. 495-504.

[12] Khatami, S.M., et al., *An ANN-Based Approach for Prediction of Sufficient Seismic Gap between Adjacent Buildings Prone to Earthquake-Induced Pounding.* Applied Sciences, 2020. **10**(10): p. 3591.

[13] Khatami, S.M., et al., *Verification of Formulas for Periods of Adjacent Buildings Used to Assess Minimum Separation Gap Preventing Structural Pounding during Earthquakes.* Advances in Civil Engineering, 2019. **2019**: p. 9714939.

[14] Favvata, M.J., *Minimum required separation gap for adjacent RC frames with potential inter-story seismic pounding.* Engineering Structures, 2017. **152**(Supplement C): p. 643-659.

[15] Cole, G., et al., *Building pounding state of the art: Identifying structures vulnerable to pounding damage*, in *NZSEE Conference*. 2010, New Zealand Society for Earthquake Engineering Inc.: New Zealand.

[16] Jeng, V. and W.L. Tzeng, *Assessment of seismic pounding hazard for Taipei City.* Engineering Structures, 2000. **22**(5): p. 459-471.

[17] EC201, *Egyptian Code for Calculating Loads and Forces in Structural Work and Masonry (Code N 201–Ministerial Decision 431/2011)*. 2012 (in Arabic), Housing and Building National Research Center (HBRC) Ministry of Housing, Utilities and Urban Planning

[18] EC-203, *Egyptian Code for the Design and Construction of Concrete Structures*. 2017.

[19] McKenna, F., G. Fenves, and M. Scott. *Open system for earthquake engineering simulation*. University of California, Berkeley, Ca 2000; Available from: http://OpenSees.berkeley.edu.

[20] Mondal, G. and S.K. Jain, *Lateral stiffness of masonry infilled reinforced concrete (RC) frames with central opening.* Earthquake Spectra, 2008. **24**(3): p. 701-723.

[21] Scott, M.H. and K.L. Ryan, *Moment-Rotation Behavior of Force-Based Plastic Hinge Elements.* Earthquake Spectra, 2013. **29**(2): p. 597-607.

[22] Scott, M. and G. Fenves, *Plastic Hinge Integration Methods for Force-Based Beam–Column Elements.* Journal of Structural Engineering, 2006. **32**(2): p. 244-252.

[23] Fragiadakis, M. and M. Papadrakakis, *Modeling, analysis and reliability of seismically excited structures: computational issues.* International journal of computational methods, 2008. **5**(04): p. 483-511.

[24] Kent, D.C. and R. Park, *Flexural members with confined concrete.* Journal of the Structural Division, 1971. **97**(7): p. 1969-1990.

[25] Menegotto, M. and P. Pinto. *Method of Analysis for Cyclically Loaded RC Frames Including Changes in Geometry and Non-elastic Behaviour of Elements Under Combined Normal Force and Bending*. in *Proc., Iabse Symp. Of Resistance and Ultimate Deformability of Structures Acted on by Welldefined Repeated Loads*. 1973. Libson, Portugal: International Association of Bridge and Structural Engineering.

[26] Filippou, F.C., E.P. Popov, and V.V. Bertero, *Effects of bond deterioration on hysteretic behavior of reinforced concrete joints.* 1983.

[27] Mohamed, H. and X. Romão, *Analysis of the performance of strut models to simulate the seismic behaviour of masonry infills in partially infilled RC frames.* Engineering Structures, 2020. **222**: p. 111124.

[28] Mohamed, H. and X. Romão, *Robust Calibration of Macro-Models for the In-Plane Behavior of Masonry Infilled RC Frames.* Journal of Earthquake Engineering, 2018: p. 1-27.

[29] Mohamed, H. and X. Romão. *Simplified modelling of in-plane behaviour of masonry infilled RC frames under seismic loading: advantages and barriers*. in *The 16th European Conference on Earthquake Engineering*. 2018. Thessaloniki, Greece.

[30] Anagnostopoulos, S.A., *Pounding of buildings in series during earthquakes.* Earthquake Engineering & Structural Dynamics, 1988. **16**(3): p. 443-456.

[31] Muthukumar, S. and R. DesRoches, *A Hertz contact model with non-linear damping for pounding simulation.* Earthquake Engineering & Structural Dynamics, 2006. **35**(7): p. 811-828.

[32] Azevedo, J. and R. Bento. *Design criteria for buildings subjected to pounding*. in *Eleventh World Conference on Earthquake Engineering, Acapulco, Mexico*. 1996.

[33] Mackie, K.R. and B. Stojadinović, *Comparison of Incremental Dynamic, Cloud, and Stripe Methods for Computing Probabilistic Seismic Demand Models.* Structures Congress 2005: p. 1-11.

[34] Scozzese, F., E. Tubaldi, and A. Dall'Asta, *Assessment of the effectiveness of Multiple-Stripe Analysis by using a stochastic earthquake input model.* Bulletin of Earthquake Engineering, 2020. **18**(7): p. 3167-3203.

[35] Bradley, B.A., *Practice-oriented estimation of the seismic demand hazard using ground motions at few intensity levels.* Earthquake Engineering & Structural Dynamics, 2013: p. n/a-n/a.

[36] Araújo, M., et al., *Code-based record selection methods for seismic performance assessment of buildings.* Earthquake Engineering & Structural Dynamics, 2016. **45**(1): p. 129-148.

[37] Martins, L. and V. Silva. *A global database of vulnerability models for seismic risk assessment*. in *16th European conference on earthquake engineering. Thessaloniki, Greece*. 2018.

[38] Mohamed, H. and X. Romão. *Seismic fragility analysis of RC frames with masonry infills*. in *16ECEE*. 2018. Thessaloniki, Greece.

[39] FEMA-273, *NEHRP Guidelines for the seismic rehabilitation of buildings*, in *Federal Emergency Management Agency*. 1997: Washigton D.C., Maryland, USA.

[40] Rossetto, T. and A. Elnashai, *Derivation of vulnerability functions for European-type RC structures based on observational data*. Engineering Structures, 2003. **25**(10): p. 1241-1263.

[41] Ghobarah, A. *On drift limits with different damage levels*. in *Proceedings of International Workshop on Performance-Based Seismic Design Concepts and Implementation, June 28th–July 1st*. 2004.

[42] Rossetto, T. and A. Elnashai, *A new analytical procedure for the derivation of displacement-based vulnerability curves for populations of RC structures.* Engineering Structures, 2005. **27**(3): p. 397-409.

[43] Vamvatsikos, D. and C.A. Cornell, *Developing efficient scalar and vector intensity measures for IDA capacity estimation by incorporating elastic spectral shape information.* Earthquake Engineering & Structural Dynamics, 2005. **34**(13): p. 1573-1600.

[44] Aschheim, M., E. Hernández-Montes, and D. Vamvatsikos, *Design of Reinforced Concrete Buildings for Seismic Performance: Practical Deterministic and Probabilistic Approaches*. 2019: Crc Press.

[45] Mohamed, H., *Seismic risk assessment of reinforced concrete frames with masonry infill*, in *Civil Engineering Department*. 2017, University of Porto: Porto.

تقييم الضعف الزلزالي لإطارات الخرسانية الموجودة في نهاية صف من المباني ذات منسوب بلاطة خرسانية واحد باستخدام تحليل متعدد الشرائح.

الملخص العربى

أثناء حدوث الزلازل تبدأ المباني المتجاورة في الاهتزاز في اتجاهات مختلفة مما يؤدي إلى تصادمها بعضها البعض مما يتسبب في أضرار جسيمة في ظاهرة تعرف باسم القصف الزلزالي. تقوم هذه الدراسة بتحليل آثار القصف على العديد من حالات الدراسة التي تمثل أحد التكوينات الانشائية الحرجة الموجودة في تصنيف المباني المصرية وهي المباني الموجودة في نهاية صف من المباني. لتقييم الأداء الإنشائي للمباني محل الدراسة على اساس احتمالي، تم اعتماد نهج التحليل متعدد الشرائح (MSA) لتقليل الجهد الحسابي المطلوب باستخدام خمسين سجل زلازلي. تمت مقارنة الأداء الهيكلي الذي تم الحصول عليه للحالات المدروسة (معبراً عنه في شكل منحنيات هشاشة) مع الحالات المرجعية المقابلة (أي المباني التي لا تحتوي على مبانٍ مجاورة). اعطت النتائج نظرة شاملة لنوع آليات الفشل التي تتحكم في الانهيار العام للحالات المدروسة. ايضا تم استنتاج النموذج الرياضي للمنحنيات الهشاشة لحالات حدود مختلفة لإعطاء صورة كاملة على سلوك المباني المدوسة في مستويات مختلفة من الاداء. علاه على ذلك سلطت النتائج الضوء على الفروق الرئيسية بين الأداء المتوقع لحالات القصف مقارنة بالحالات المرجعية. أخيرًا، تشير النتائج إلى أهمية تأثير القصف على الأداء العام للحالات المدروسة، لذلك يجب أن تأخذ دراسات تقييم مخاطر الزلازل واسعة النطاق في الاعتبار تأثير القصف الزلزالي